Cell PRESS
Open ACCESS

Cell Reports
Report

A Reversible Gene-Targeting Strategy Identifies Synthetic Lethal Interactions between MK2 and p53 in the DNA Damage Response In Vivo

Sandra Morandell,[1] H. Christian Reinhardt,[1,2,3] Ian G. Cannell,[1] Jacob S. Kim,[1] Daniela M. Ruf,[1] Tanya Mitra,[1,9] Anthony D. Couvillon,[4] Tyler Jacks,[1,5,6] and Michael B. Yaffe[1,5,7,8,*]

[1]David H. Koch Institute for Integrative Cancer Research, Massachusetts Institute of Technology, Cambridge, MA 02139, USA
[2]Cologne Excellence Cluster on Cellular Stress Response in Aging-Associated Diseases, University of Cologne, 50674 Cologne, Germany
[3]Division I Hematology/Oncology, Department of Internal Medicine, University Hospital of Cologne, 50937 Cologne, Germany
[4]Cell Signaling Technology, Danvers, MA 01923, USA
[5]Department of Biology, Massachusetts Institute of Technology, Cambridge, MA 02139, USA
[6]Howard Hughes Medical Institute, Massachusetts Institute of Technology, Cambridge, MA 02139, USA
[7]Department of Biological Engineering, Massachusetts Institute of Technology, Cambridge, MA 02139, USA
[8]Department of Surgery, Beth Israel Deaconess Medical Center, Harvard Medical School, Boston, MA 02215, USA
[9]Deceased
*Correspondence: myaffe@mit.edu

http://dx.doi.org/10.1016/j.celrep.2013.10.025

SUMMARY

A fundamental limitation in devising new therapeutic strategies for killing cancer cells with DNA damaging agents is the need to identify synthetic lethal interactions between tumor-specific mutations and components of the DNA damage response (DDR) in vivo. The stress-activated p38 mitogen-activated protein kinase (MAPK)/MAPKAP kinase-2 (MK2) pathway is a critical component of the DDR network in p53-deficient tumor cells in vitro. To explore the relevance of this pathway for cancer therapy in vivo, we developed a specific gene targeting strategy in which Cre-mediated recombination simultaneously creates isogenic MK2-proficient and MK2-deficient tumors within a single animal. This allows direct identification of MK2 synthetic lethality with mutations that promote tumor development or control response to genotoxic treatment. In an autochthonous model of non-small-cell lung cancer (NSCLC), we demonstrate that MK2 is responsible for resistance of p53-deficient tumors to cisplatin, indicating synthetic lethality between p53 and MK2 can successfully be exploited for enhanced sensitization of tumors to DNA-damaging chemotherapeutics in vivo.

INTRODUCTION

DNA damage signaling and checkpoint control pathways are among the most commonly mutated networks in human tumors (Negrini et al., 2010). Although dampening of DNA repair pathways and suppression of DNA damage signaling networks that arrest the cell cycle after genotoxic stress enhances genomic instability during tumor development, it also furnishes an "Achilles' heel" for anticancer therapy. Emerging data suggest that synthetic lethal interactions between mutated oncogenes or tumor suppressor genes with molecules involved in the DNA damage response could be used to preferentially kill cancer cells by exploiting dependencies that are not shared by normal tissue (Lord and Ashworth, 2012; Morandell and Yaffe, 2012; Reinhardt et al., 2009).

In response to DNA damage, cells activate complex signaling networks that mediate DNA repair and cell cycle arrest or, if the damage is extensive, trigger apoptosis (Ciccia and Elledge, 2010). Two canonical protein kinase pathways in both normal and cancer cells arrest the cell cycle in response to damaged DNA: the ATR-Chk1 and the ATM-Chk2 pathway. We previously identified a third cell-cycle checkpoint pathway mediated by the stress-activated protein kinases p38 mitogen-activated protein kinase (MAPK) and its substrate MAPKAP kinase-2 (MK2). This MK2 pathway is critical for arresting the cell cycle after genotoxic stress, including cisplatin-induced DNA crosslinks and topoisomerase-inhibitor-induced DNA strand breaks only in tumor cells that lack functional p53, whereas MK2 is dispensable for checkpoint function in p53-proficient nontumor cells (Manke et al., 2005; Reinhardt et al., 2007). Importantly, both the ATR-Chk1 pathway and the p38-MK2 pathway are required for effective cell-cycle checkpoint function in the absence of p53 (Reinhardt et al., 2010). Under this condition, cytoplasmic MK2 orchestrates a cell-cycle checkpoint through the posttranscriptional regulation of gene expression by modulating the function of RNA-binding proteins. MK2 phosphorylates the RNA-binding protein hnRNPA0, inducing its association with and stabilization of the mRNA of Gadd45α, a known cyclin-dependent kinase inhibitor (Reinhardt et al., 2010). In addition, MK2 induces miR-34c

in response to DNA damage in cells that lack p53. MiR-34c then represses the translation of c-Myc to promote S-phase arrest (Cannell et al., 2010).

Our previous observations based on immortalized tumor cell lines and xenograft tumors in nude mice (Reinhardt et al., 2007, 2010) suggest that therapeutic targeting of MK2 might be a useful strategy to enhance killing of p53-defective tumors by DNA-damaging chemotherapy in situ. Normal host tissues are expected to be protected from the enhanced genotoxicity of MK2 inhibition due to the presence of functional p53.

To directly test this hypothesis and study the role of MK2 in tumor development and chemotherapeutic treatment in vivo, we generated a conditional knockout mouse in which we can simultaneously generate MK2-expressing and MK2-null tumors within a single animal. Here, we use this approach to study the role of MK2 in a well-established autochthonous model of non-small-cell lung cancer (NSCLC) (Jackson et al., 2001, 2005; Johnson et al., 2001) that closely recapitulates the histopathology and therapeutic response of the human disease. In this model, the expression of oncogenic $Kras^{G12D}$ (found in ~30% of human NSCLCs) initiates the formation of lung adenomas in mice that are either wild-type or deficient for *TP53* (*p53*; mutated in ~50% of human NSCLCs) and differ only in MK2 expression status. This ability to generate otherwise genetically identical tumors in individual mice that differ in only a single genetic locus and monitor their response to treatment allows a direct in vivo analysis of synthetic lethal interactions in a solid tumor model.

RESULTS

A Cre-Versible Strategy for Comparing Wild-Type and Knockout Tumors in a Single Animal

To simultaneously study MK2-proficient and MK2-deficient tumors within a single animal, we generated a new mouse model with a stochastic reversible MK2 knockout phenotype. In this inducible model, Cre-mediated recombination switches exon 2 reversibly from an MK2-expressing state to an MK2 inactive state and back. To generate mice carrying "Cre-versible" alleles of MK2 ($MK2^{CV}$), we constructed a targeting vector with *LoxP* sites, the recognition sites for Cre-recombinase, flanking exon 2 in opposing orientations (Figures 1A and S1A). Upon Cre-mediated recombination, the region flanked by the *LoxP* sites is inverted rather than excised as in classical conditional alleles, where the *LoxP* sites are oriented in the same direction (Tronche et al., 2002). Consequently, exon 2 can invert reversibly from an MK2-expressing orientation ($MK2^{+CV}$) to an MK2-null orientation ($MK2^{-CV}$) and back as long as Cre is active in the cell (Figure 1B). Inversion of exon 2 disrupts the splice donor and acceptor sites, resulting in an mRNA product with exon 1 directly fused to exon 3. This leads to a frame shift and a STOP codon in the beginning of exon 3, creating a highly truncated reading frame that is not translated into functional MK2 proteins (i.e., loss of both the 46 KDa and 42 KDa isoforms corresponding to Uniprot P49137-1 and P49137-2 for human MK2).

In vitro infection of mouse embryonic fibroblasts (MEFs) from homozygous mice carrying two copies of the MK2 Cre-versible allele ($MK2^{CV/CV}$) with adenoviral Cre-recombinase (Adeno-Cre) confirmed the Cre-mediated inversion of exon 2, shown by PCR (Figure 1C) and sequencing of cDNA fragments obtained from RNA of Adeno-Cre-infected $MK2^{CV/CV}$ MEFs (Figures S1B and S1C). MK2 protein levels were strongly decreased in $MK2^{CV/CV}$ MEFs upon Adeno-Cre as a result of the inversion of exon2 in a significant subset of infected cells (Figure 1D). This Cre-versible allele, when used in combination with murine tumor models, allows altered MK2 expression in a tissue-specific manner and at the same time generates a mixture of MK2-proficient and MK2-deficient cells in any tissue where Cre-recombinase is active. As a consequence, tumors that are genetically identical, except for MK2 expression, can be directly compared in vivo in single animals.

MK2-Expressing and MK2-Deficient Tumors Develop in a Murine Autochthonous Model of NSCLC

To explore the role of MK2 in cancer development, progression, and response to DNA-damaging chemotherapy in an epithelial tumor type in vivo, we focused on a well-established autochthonous mouse model of NSCLC. $MK2^{CV/CV}$ mice were crossed against mice containing either wild-type *TP53* ($p53^{+/+}$) or biallelic floxed *TP53* ($p53^{flox/flox}$) in combination with a $Kras^{G12D}$ allele preceded by a *LoxP*-STOP-*LoxP* cassette (Jackson et al., 2001, 2005; Johnson et al., 2001) in the endogenous *Kras* locus (Figure S2A). After intratracheal administration of a Cre-recombinase-expressing adenovirus (Adeno-Cre), the expression of oncogenic $Kras^{G12D}$ initiates the development of adenomas at 100% penetrance even in a wild-type *p53* background (Jackson et al., 2001; Johnson et al., 2001), whereas concomitant loss of *p53* shortens latency and leads to advanced histopathology (Jackson et al., 2005), including adenocarcinomas. Importantly, because Adeno-Cre does not integrate into the genome of infected cells, the MK2 expression state that is established by transient Cre expression in the tumor-initiating cell is maintained throughout further tumor evolution. Thus, this Cre-versible mouse model allows comparison of the initiation and/or progression of otherwise genetically identical MK2-expressing and MK2-deficient lung tumors within the same animal and, simultaneously, allows the effects of DNA-damaging chemotherapy to be directly studied in each tumor type.

Figure 2A gives an overview over the different mouse lines generated for this study. In $MK2^{+/+}$ mice, both the normal lung tissue and all tumors express MK2 (MK2+) as shown by immunohistochemistry for MK2 expression (Figure 2B for $p53^{flox/flox}$ mice and Figure S2B for $p53^{+/+}$ mice). In contrast, a subset of $MK2^{CV/CV}$ tumor-initiating cells lose expression of MK2 upon Cre-mediated inversion of exon 2 on both $MK2^{CV}$ alleles, leading to a mixture of MK2-positive (MK2+) and MK2-negative tumors (MK2−) within the same animal (Figures 2C for $p53^{flox/flox}$ mice and Figure S2C for $p53^{+/+}$ mice). (Because homozygous $MK2^{+CV/+CV}$ and heterozygous $MK2^{+CV/-CV}$ tumors both stain positive for MK2, they are grouped together as MK2+ tumors.) In addition, we observed intense MK2 staining in stromal cells surrounding and infiltrating the tumors (Figure 2C, insert). The histological appearance of both MK2-expressing and MK2-null tumors was comparable to tumors described for the original $Kras^{LSL-G12D}$;$p53^{+/+}$ (Jackson et al., 2001; Johnson et al., 2001) and $Kras^{LSL-G12D}$; $p53^{flox/flox}$ models (Jackson et al., 2005).

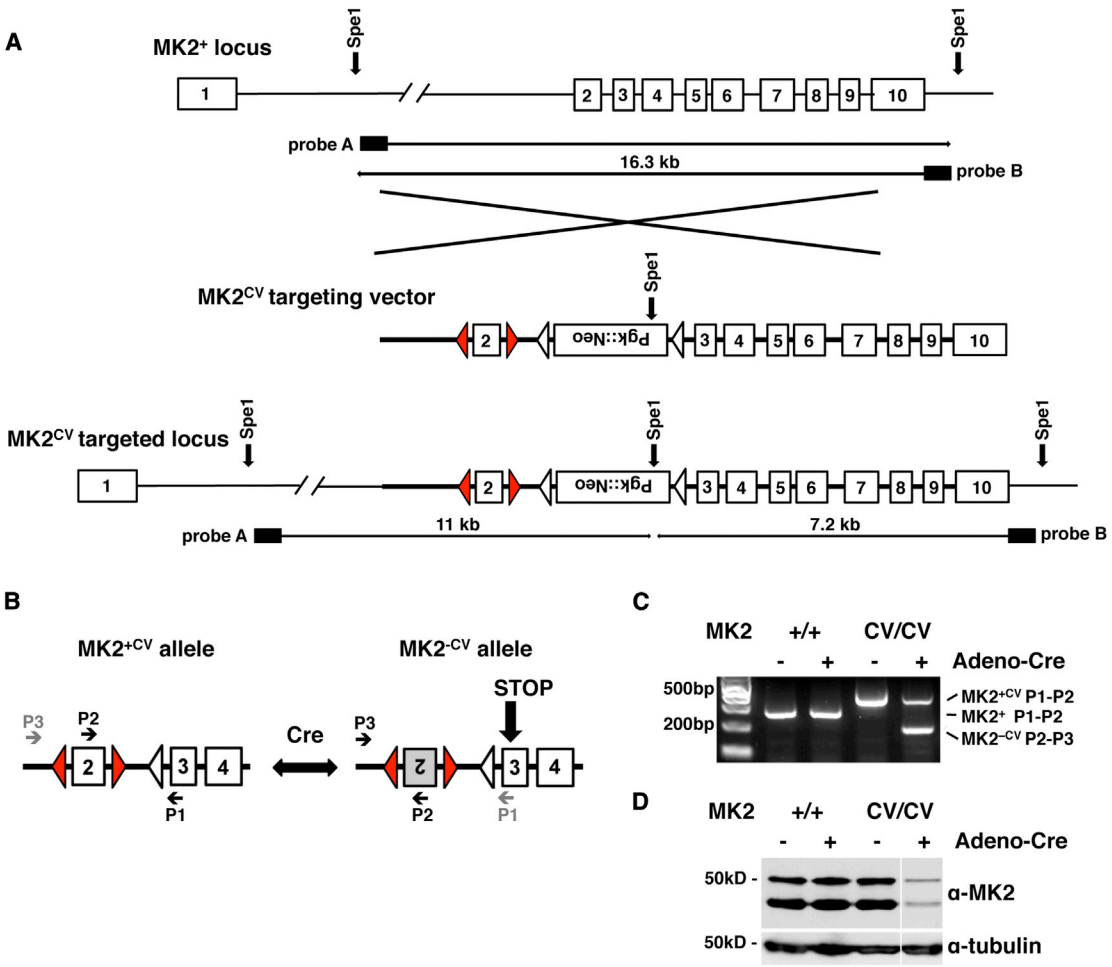

Figure 1. A Cre-Versible Strategy for Comparing Wild-Type and Knockout Tumors in a Single Animal

(A) Schematic representation of the wild-type MK2 (*MK2*$^{+}$) genomic locus (top), the MK2 Cre-versible (*MK2*^{CV}) targeting vector (middle), and the targeted *MK2*^{CV} genomic locus (bottom). *MK2* exons 1–10, white boxes. *LoxP* sites, red triangles; *FRT* sites, white triangles. The final targeting construct consists of 2.7 kB of the 5′ flanking sequence before exon 2, the first *LoxP* site, exon 2 followed by a second *LoxP* site in reverse complement sequence as the first *LoxP* site, a *FRT*-Pgk::Neo-*FRT* cassette, and exons 3–10. Positions of SpeI restriction sites and probes A and B for Southern blot detection of targeted embryonic stem cell are highlighted.

(B) Diagram of exons 2–4 of the *MK2*^{CV} allele after FlPe-mediated excision of the Pgk::Neo-cassette: upon Cre-mediated recombination, exon 2 can invert reversibly between the MK2-expressing (*MK2*$^{+CV}$) and the MK2-negative orientation (*MK2*$^{-CV}$). Inversion of exon 2 results in a STOP codon early in exon 3. P1, P2, and P3 indicate primers for genotyping.

(C) PCR analysis of *MK2*$^{+/+}$ and *MK2*$^{CV/CV}$ MEFs infected with adenoviral Cre-recombinase (Adeno-Cre) or control; positions for primers P1, P2, and P3: (B). *MK2*$^{+}$ or *MK2*$^{+CV}$ alleles yield 241 bp or 333 bp PCR products with primers P1 and P2, respectively. The inverted *MK2*$^{-CV}$ allele yields a 190 bp PCR product with primers P2 and P3; the distance between primers P1 and P3 is too long to form a product.

(D) Western blot of *MK2*$^{+/+}$ and *MK2*$^{CV/CV}$ MEFs infected with Adeno-Cre or control: *MK2*$^{+}$ and *MK2*$^{+CV}$ alleles encode for two MK2 protein isoforms with 46 kD and 42 kD, respectively. No protein product is formed from the *MK2*$^{-CV}$ allele. γ-tubulin, loading control.

When we compared the initial onset of tumors, we observed that *MK2*$^{CV/CV}$ mice develop tumors at the same latency and frequency as *MK2*$^{+/+}$ mice (Figure S2D). Whereas the MK2 expression status has no influence on tumor initiation, tumors in *p53*$^{flox/flox}$ mice had progressed further at earlier time points than tumors with wild-type p53, as the loss of p53 is known to promote the progression of *Kras*^{G12D}-induced lung adenocarcinomas (Jackson et al., 2005). Therefore, for *p53*$^{flox/flox}$ mice, 6 weeks was chosen as the earliest time point for quantification of tumor areas, whereas 9 weeks was chosen for mice with wild-type p53. At these early time points, the total tumor burden in both models was similar with 11% of the lung area occupied by tumor for both *MK2*$^{+/+}$ and *MK2*$^{CV/CV}$ in the p53-deficient model (*Kras*$^{G12D/+}$;*p53*$^{\Delta/\Delta}$) (Figure S2D). In a p53 wild-type background (*Kras*$^{G12D/+}$;*p53*$^{+/+}$), 11% of lung area in *MK2*$^{+/+}$ mice and 9% in *MK2*$^{CV/CV}$ mice were occupied by tumors (Figure S2D). Thus, tumor initiation in this autochthonous model of NSCLC is independent of the tumor MK2 status.

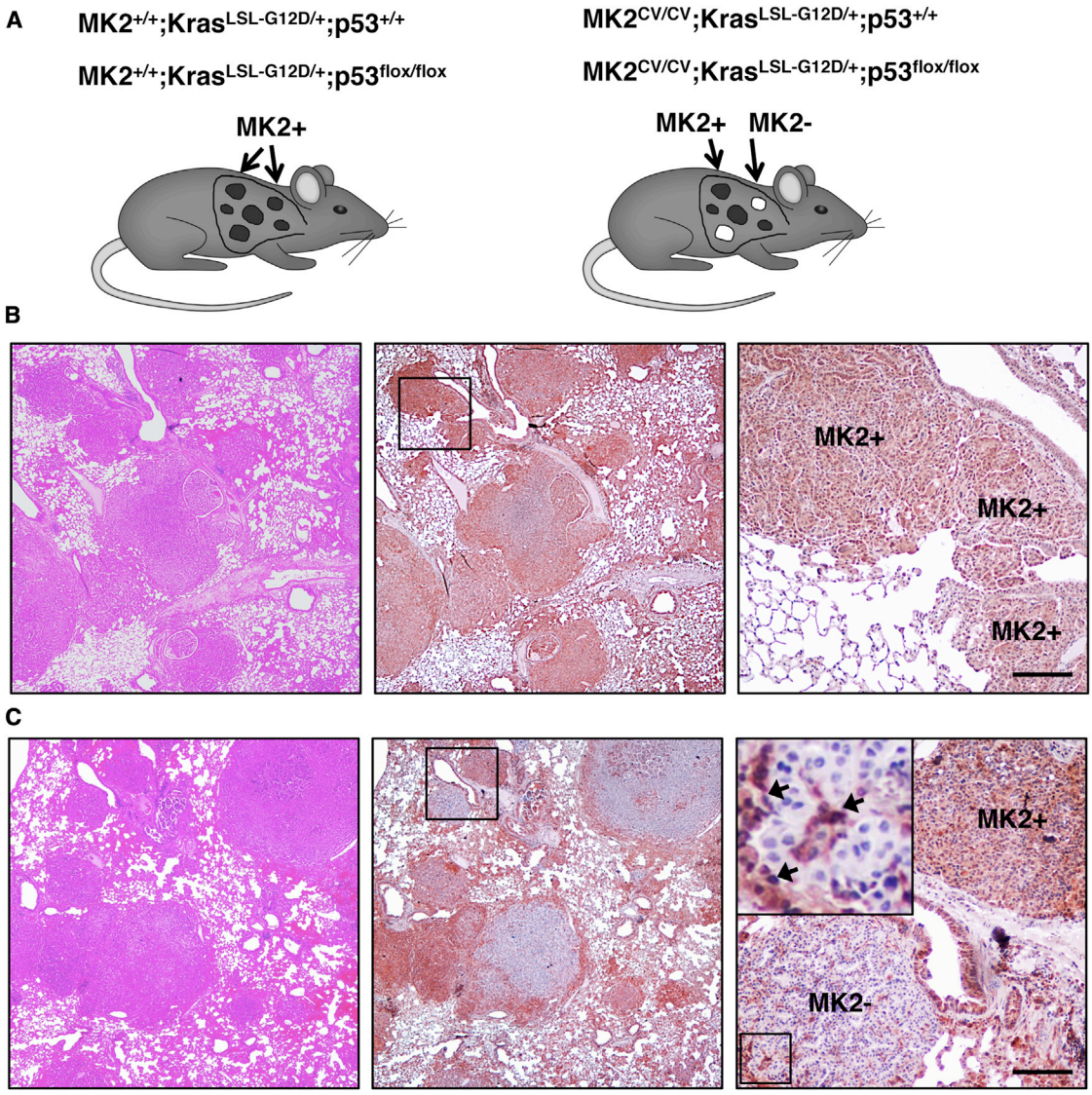

Figure 2. MK2-Expressing and MK2-Deficient Tumors Develop in a Murine Autochthonous Model of NSCLC

(A) Combinations of *MK2*, *Kras*, and *p53* alleles used in this study: $MK2^{+/+}$ or $MK2^{CV/CV}$ mice harbor one copy of the $K\text{-}ras^{LSL\text{-}G12D}$ allele in a wild-type p53 background ($p53^{+/+}$) or they contain two copies of the $p53^{flox}$ allele ($p53^{flox/flox}$). After Cre-mediated recombination, the respective tumor MK2 status in $MK2^{+/+}$ and $MK2^{CV/CV}$ mice is indicated as "MK2+" for MK2-expressing tumors and "MK2−" for MK2-negative tumors, exclusively found in $MK2^{CV/CV}$ mice.

(B) Tumors from a $MK2^{+/+}$;$Kras^{LSL\text{-}G12D/+}$;$p53^{fl/fl}$ mouse at the experimental endpoint were stained with hematoxilin and eosin (left) or by IHC for MK2 (brown staining, middle). Right: close-up of three MK2+ tumors. The scale bar represents 50 μm.

(C) Tumors from a $MK2^{CV/CV}$;$Kras^{LSL\text{-}G12D/+}$;$p53^{fl/fl}$ mouse at the experimental endpoint, stained as in (B). Right: close-up of MK2+ tumor (brown staining) and MK2− tumor (blue counterstain only). MK2-expressing stroma cells infiltrate and surround an MK2-negative tumor (arrows). In (B) and (C), the experimental endpoint corresponds to 20% basal weight loss of tumor-bearing animals.

MK2-Deficient Tumors Dominate the Total Tumor Burden Over Time in a Manner That Is Dependent on the Loss of p53

Whereas the presence or absence of MK2 expression has no effect on tumor initiation, it did appear to affect tumor progression. For p53-null tumors, the total tumor burden of MK2+ and MK2− tumors combined progressed over time from 11% at 6 weeks to 45% of total lung area (Figure 3A). In p53-proficient tumors, the tumor burden increased from 9% after 9 weeks to 28% of total lung area (Figure 3C). When we separated the tumors according to MK2-expression, we observed that, over time, the increase of MK2/p53 double knockout (DKO) tumor areas (MK2−) outpaced that of MK2-expressing tumors (MK2; Figure 3A). This became more obvious when we quantified the relative lung area occupied by MK2+ or MK2− tumors as percentage of total tumor burden. At the earliest time points, MK2+ tumors account for 84% of the total tumor area in both $p53^{fl/fl}$ and $p53^{+/+}$ mice, whereas 16% of tumors are

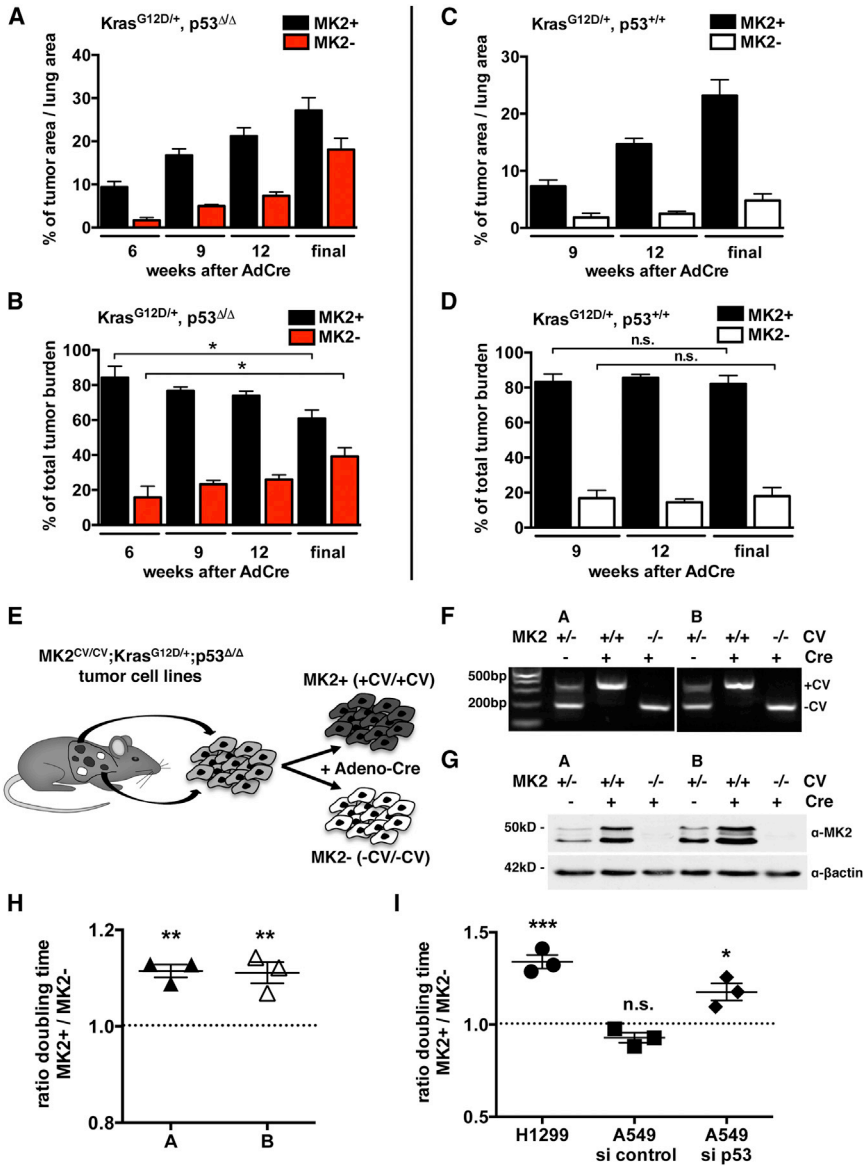

Figure 3. MK2-Deficient Tumors Dominate the Total Tumor Progression Over Time in a Manner That Is Dependent on the Loss of p53

(A and B) Quantification of $MK2^{CV/CV}$;$Kras^{G12D/+}$;$p53^{\Delta/\Delta}$ tumors at weeks 6, 9, and 12 after tumor induction and at experimental endpoint (final): MK2+ and MK2− tumor areas are shown as percentage of total lung area (A) and relative percentages of total tumor burden (B). (A–D): n = 4 to 5 mice per time point; *p ≤ 0.02; error bars indicate SEM.

(C and D) Quantification of $MK2^{CV/CV}$;$K\text{-}ras^{G12D/+}$;$p53^{+/+}$ tumors at weeks 9 and 12 after tumor induction and at experimental endpoint (final): MK2+ and MK2− tumor areas shown as percentage of total lung area (C) and relative percentages of total tumor burden (D). n.s., not significant.

(E) Generation of isogenic MK2+ and MK2− $Kras^{G12D/+}$;$p53^{\Delta/\Delta}$ murine NSCLC cell lines.

(F) PCR analysis of two isogenic MK2+ and MK2− murine NSCLC cell line pairs, A and B, before (−Cre) and after infection with Adeno-Cre (+Cre). Initial cell lines harbored one MK2-expressing (+CV) and one MK2-negative (−CV) allele. After Cre infection, selected clones inverted one allele, resulting in homocygous $MK2^{+CV/+CV}$ (MK2+) or $MK2^{-CV/-CV}$ (MK2−) cells.

(G) Western blot of isogenic MK2+ and MK2− murine NSCLC cell line pairs. β-actin, loading control.

(H) Ratio of doubling times between MK2+ and MK2− isogenic cell lines A and B. (H and I): n = 3 independent experiments; *p < 0.02; **p < 0.008; ***p < 0.001; error bars represent SEM.

(I) Ratio of doubling times between H1299 cells stably expressing a control hairpin (MK2+) or hairpin against MK2 (MK2−) and A549 cells with or without small interfering RNA (siRNA) against MK2 in combination with or without siRNA against 53.

MK2− (Figures 3B and 3D). Interestingly, MK2/p53 DKO tumors subsequently accounted for 23% of total tumor burden after 9 weeks, 26% after 12 weeks, and 39% of the total tumor burden at the experimental endpoint. In striking contrast, in the presence of wild-type p53, the proportion of MK2− tumors remained constant over time (Figures 3B and 3D).

This increase in MK2/p53 DKO tumor burden during tumor progression could be caused by enhanced proliferation, by reduced cell death, or by a combination of these two mechanisms. To examine this, we generated tumor cell lines from $MK2^{CV/CV}$;$Kras^{LSL\text{-}G12D/+}$;$p53^{flox/flox}$ mice. To avoid heterogeneity in cell lines from different tumors, we used the Cre-versible MK2 allele to create isogenic MK2+ and MK2− clones from the same parental cell lines by reinfecting single-cell clones in culture with Adeno-Cre (Figure 3E). Two pairs of NSCLC cell lines, A and B, were chosen for further study. For both cell lines, we generated one MK2+ clone with both alleles oriented in the MK2-expressing orientation ($MK2^{+CV/+CV}$) and one MK2− clone with both alleles inverted to the MK2-negative orientation ($MK2^{-CV/-CV}$) (Figures 3F and 3G).

Comparison of proliferation rates revealed that MK2/p53-DKO murine NSCLC cells doubled on average 11% faster than their isogenic MK2-proficient counterparts (Figure 3H). To investigate whether this MK2-dependent suppression of proliferation in p53-deficient cells was unique to murine lung tumors, we knocked down MK2 in two human NSCLC cell lines. In p53-deficient H1299 cells, small hairpin RNA knockdown of MK2 shortened their doubling time by 34% (Figure 3I). In contrast, in p53-proficient A549 cells, the doubling time was largely independent on MK2 expression (Figure 3I). However, combined knockdown of p53 and MK2 in these cells shortened their doubling time by 18% relative to p53-knockdown/MK2-expressing A549 cells (Figure 3I).

These data clearly indicate that the combined loss of MK2 and p53 accelerates proliferation both in vitro in murine and human

NSCLC cell lines and in vivo in a murine autochthonous model of NSCLC. When integrated over time, these moderate differences in cell proliferation result in a progressive increase in MK2-negative tumor burden over MK2-expressing tumors. In contrast, no such difference exists between MK2+ and MK2− tumors that retain p53 function.

MK2 Is Required for Survival after DNA Damage in p53-Deficient Lung Tumor Cells

We have previously shown in vitro that U2OS and HeLa tumor cell lines with a defective p53 pathway are critically dependent upon a cytoplasmic p38/MK2 pathway for prolonged G_2/M and G_1/S checkpoint maintenance in response to chemotherapy-induced DNA damage (Reinhardt et al., 2007, 2010). Platinum-based compounds are widely used as frontline chemotherapeutic agents for the treatment of NSCLC patients (Azzoli et al., 2009). We therefore investigated if targeting of MK2 could be a useful strategy to preferentially enhance DNA-damage-induced killing of p53-defective NSCLC cells derived from primary tumors.

Isogenic MK2+ and MK2− murine NSCLC tumor cells were treated with cisplatin and assayed for clonogenic survival. MK2− cells showed a strong increase in cisplatin sensitivity (Figure 4A). Whereas, on average, 30% of MK2+ cells survive treatment with 5 μM cisplatin, loss of MK2 reduced the survival to between 13% (cell line A) and 24% (cell line B) survival. Treatment with 10 μM cisplatin resulted in similar differences in survival between the MK2+ and MK2− cell lines. This same chemosensitizing effect upon loss of MK2 is observed in the human p53-deficient cell line H1299 (Figure 4B). Knockdown of MK2 in this cell line reduced survival following treatment with 5 μM cisplatin to 19% compared to 33% of cells with intact MK2 levels. Significant differences in survival were also observed following treatment with 10 μM cisplatin. In striking contrast, in A549 cells with functional p53, no significant increase in chemosensitivity was observed following MK2 knockdown. Knockdown of p53 in these cells actually improved survival in the presence of MK2, whereas a combined knockdown of MK2 and p53 rendered this cell line more sensitive to cisplatin treatment, leading to a decrease in survival from 29% to 20% (Figure 4C).

To further probe the mechanism of differential chemosensitivity in more detail, we monitored the extent of apoptosis in MK2+ and MK2− cells in response to cisplatin treatment by measuring cleaved caspase 3 (CC3) levels. Interestingly, murine MK2/p53-DKO NSCLC cells (Figures 4D and 4E) as well as human H1299 cells stably knocked down for MK2 (Figures 4F and 4G) displayed a 2-fold increase in CC3 levels, even in the absence of cisplatin-induced DNA damage. Despite this, we consistently observed a net increase in the proliferation of these cells (Figures 3 and S3; see Discussion). Following cisplatin treatment, both MK2− and MK2+ cells showed enhanced cleavage of caspase 3. However, cells lacking both MK2 and p53 displayed much higher levels of CC3 in both murine NSCLC cell lines A and B (Figures 4D and 4E) and human H1299 cells (Figures 4F and 4G). In contrast, the extent of caspase 3 cleavage in cisplatin-treated p53-proficient A549 cells was independent of MK2 status (Figures 4F and 4G). These data extend our previous findings in other cell types (Reinhardt et al., 2007, 2010) and implicate MK2 inhibition as a mechanism to sensitize p53-deficient NSCLC tumor cell lines to clinically relevant chemotherapeutic treatments.

The enhanced basal rate of proliferation that we observed when murine and human NSCLC cells were depleted of both MK2 and p53 was completely lost following 5 μM cisplatin treatment (Figures S3A and S3B). After DNA damage, one of the MK2− murine NSCLC lines (cell line A) actually proliferated slower than its MK2+ counterpart, whereas for all other cell lines (cell line B, H1299, and A549), there was no statistically significant difference in relative proliferation rates after damage between MK2 + and MK2− cells. In all cell lines, the extent of cell proliferation was markedly reduced following cisplatin treatment (Figures S3C–S3G).

MK2 and p53 Codeficiency in an Autochthonous Model of NSCLC Results in Dramatic Chemosensitivity

To investigate whether these in vitro observations can be extended to the response of autochthonous p53-proficient and p53-deficient lung tumors in vivo, individual animals bearing a mixture of MK2+ and MK2− lung tumors were treated with three doses of cisplatin (*Cis*, 5 mg/kg, intraperitoneally [i.p.]) at 12, 13, and 14 weeks after tumor induction (Figure 5A). The relative ratios of MK2+ versus MK2− tumor areas in cisplatin-treated mice and vehicle-treated control mice were then compared at the experimental endpoint. In mice with p53-deficient tumors ($Kras^{G12D/+};p53^{\Delta/\Delta}$), the percentage of the total lung tumor burden composed of MK2− tumors was strongly reduced from 39% to 11% following cisplatin treatment (Figures 5B and 5C). In contrast, in a wild-type p53 tumor background ($Kras^{G12D/+};p53^{+/+}$), there was no difference in the ratio of MK2+ to MK2− lung tumor burden in response to cisplatin treatment (Figure 5D).

To investigate if this shift in in vivo tumor ratio resulted from increased apoptosis in MK2/p53 DKO tumor cells, we stained tumors for CC3 in the absence or presence of cisplatin treatment. Similar to our observations in vitro, a small but statistically significant increase in CC3-positive cells in MK2/p53 DKO tumors was seen, even in the absence of exogenous DNA damage. Importantly, however, DNA-damaging chemotherapy further enhanced this difference (Figures 5E and 5F). In contrast, cisplatin treatment of autochthonous tumors containing wild-type p53 resulted in a strong increase in CC3-positive cells, irrespective of the tumor MK2 status (Figure 5G).

DISCUSSION

Deficiency in p53 represents a difficult clinical challenge, as it is generally thought to be associated with resistance to genotoxic anticancer therapies (Rusch et al., 1995; Viktorsson et al., 2005). Therefore, novel therapeutic concepts to overcome the resistance of p53-defective neoplastic disease are urgently needed. In the present study, we identified a molecular liability of p53-defective tumors that could be therapeutically exploited. We show that, in response to genotoxic chemotherapy, MK2 is essential for the survival of NSCLC tumor cells that lack functional p53 but is dispensable in p53-proficient cells. Importantly, findings from murine and human cell lines could be extended to a

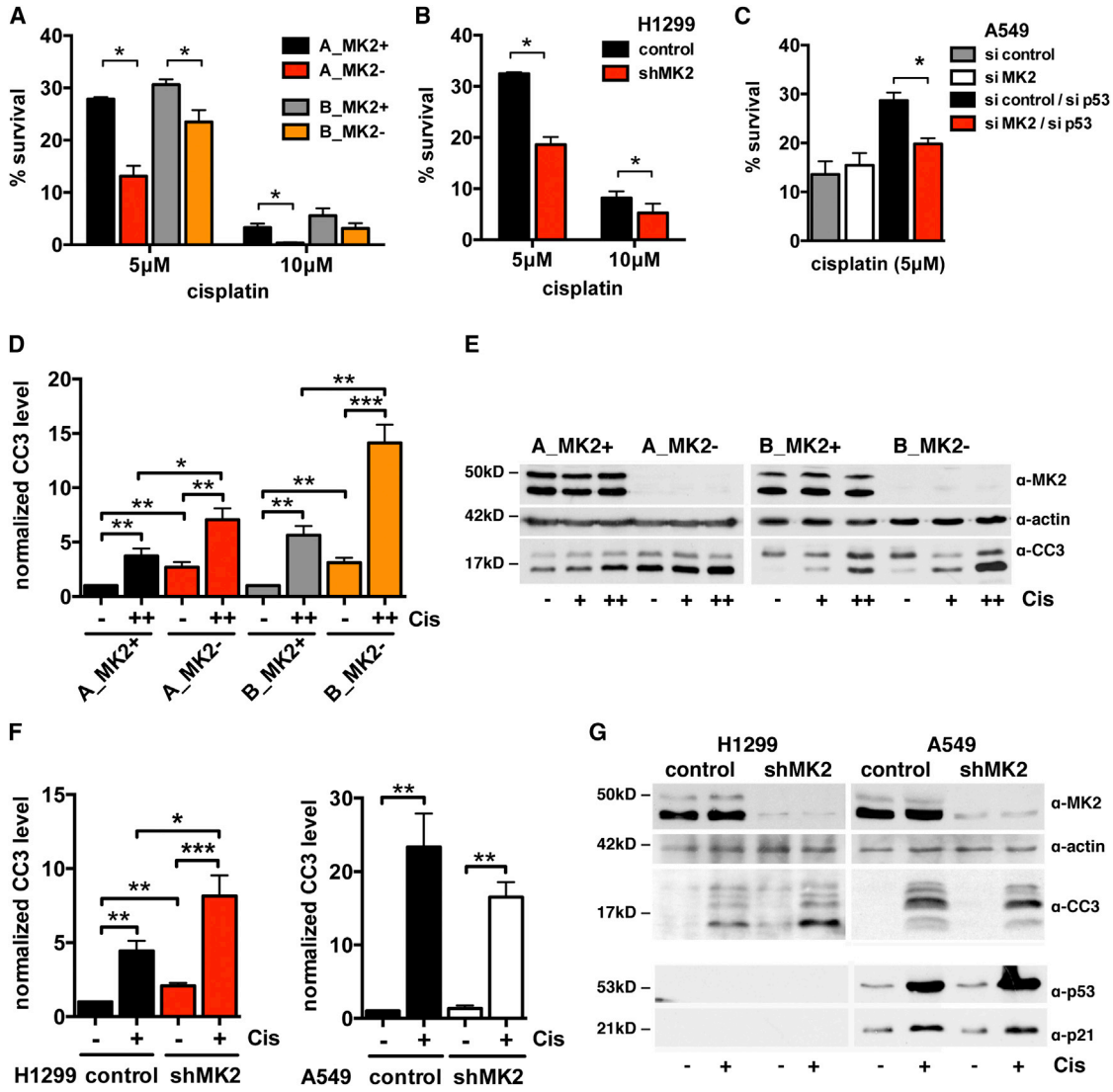

Figure 4. Loss of MK2 Results in Increased Chemosensitivity in p53-Deficient Tumor Cells In Vitro

(A) Quantification of clonogenic survival assays for isogenic MK2+ and MK2− murine NSCLC cell line pairs A and B, treated with vehicle, 5 μM, or 10 μM cisplatin. Assays were performed in triplicate for each condition and normalized to control-treated cells. (A–C): n = 3 independent experiments; *p < 0.05; error bars represent SEM.

(B and C) Quantification of clonogenic survival assays for H1299 cells (B) stably expressing a control hairpin or hairpin against MK2 and for A549 cells (C) with and without siRNA against MK2 in combination with or without siRNA against p53.

(D) Quantification of western blots for cleaved caspase 3 (CC3) levels in isogenic MK2+ and MK2− murine NSCLC cell line pairs A and B. Cells were treated with vehicle or cisplatin (+, 5 μM; ++, 10 μM) for 24 hr. (D and F): n = 5 independent experiments; A549: n = 3; *p < 0.05; **p < 0.09; ***p < 0.0008; error bars represent SEM. CC3 levels were normalized to vehicle-treated MK2+ cells.

(E) Representative western blots for CC3 and MK2 levels in murine NSCLC cell lines after cisplatin treatment. β-actin is a loading control.

(F) Quantification of western blots for CC3 in human NSCLC cell lines H1299 and A549 stably expressing a control hairpin or hairpin against MK2. Cells were treated with cisplatin (+, 10 μM) or vehicle for 24 hr.

(G) Representative western blot for CC3 and MK2 levels in human NSCLC cell lines in response to cisplatin treatment. The induction of p53 and p21 in A549 cells in response to cisplatin is shown.

mouse model of NSCLC and demonstrate, for the first time in an autochthonous cancer model in vivo, that loss of MK2 specifically sensitizes p53-deficient tumors to the DNA-damaging agent cisplatin. In stark contrast, the MK2 expression status has no effect on the treatment response of p53-proficient cancer cells. This suggests a potential for enhanced chemosensitization of p53-deficient tumors to DNA-damaging chemotherapy in vivo through synthetic lethality between p53 and MK2. Importantly, because adjacent nontumor tissue has intact p53 function, this approach could potentially increase the therapeutic window for DNA-damaging chemotherapy and can likely be applied to different tumor types.

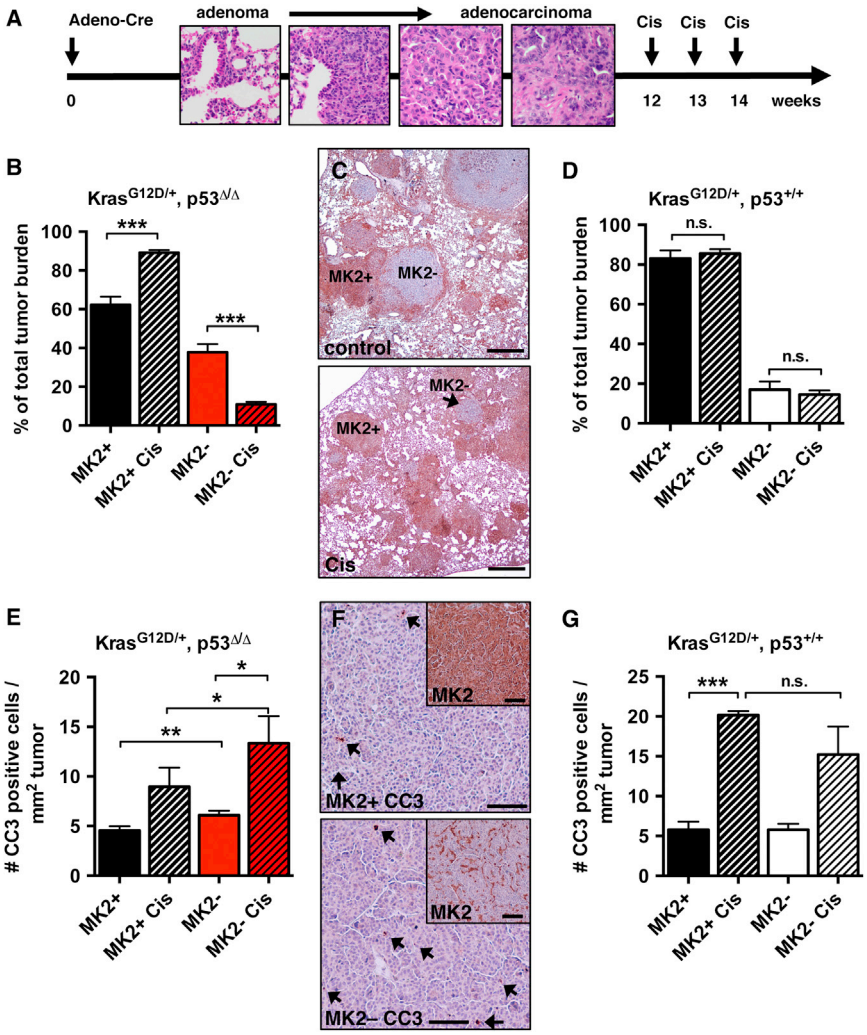

Figure 5. MK2 and p53 Codeficiency in an Autochthonous Model of NSCLC Results in Dramatic Chemosensitivity

(A) Timeline for chemotherapy treatments: mice were infected with Adeno-Cre at time 0. Cisplatin (5 mg/kg, i.p.) was given at 12, 13, and 14 weeks after tumor initiation.

(B) Relative percentages of MK2+ and MK2− *Kras*$^{G12D/+}$;*p53*$^{\Delta/\Delta}$ lung tumor areas per total tumor burden in mice vehicle-treated or treated with cisplatin at the experimental endpoint. (B–D): n = 6 mice/condition; ***p = 0.0001; error bars represent SEM.

(C) IHC of tumor-bearing lungs from *MK2*$^{CV/CV}$; *Kras*$^{LSL\text{-}G12D/+}$;*p53*$^{flox/flox}$ mice at the experimental endpoint. Top: lung from an untreated mouse. Bottom: lung from a cisplatin-treated mouse. MK2+ tumors, brown staining; MK2− tumors, blue counterstain only; one example for each tumor type labeled; scale bar represents 0.25 mm.

(D) Relative percentages of MK2+ and MK2− *Kras*$^{G12D/+}$;*p53*$^{+/+}$ lung tumor areas per total tumor burden at the experimental endpoint in mice treated with vehicle or cisplatin.

(E) Number of cleaved caspase-3 (CC3)-positive cells per mm^2 of tumor area in MK2+ and MK2− *Kras*$^{G12D/+}$;*p53*$^{\Delta/\Delta}$ lung tumors. Mice were vehicle-treated or treated with cisplatin (10 mg/kg, i.p.) 12 weeks after tumor induction. Lung tissue was harvested 48 hr later and analyzed by IHC for MK2 and CC3; n = 5 mice/condition; *p < 0.05; **p < 0.004; error bars represent SEM; n (tumors) = 222 (MK2+), 232 (MK2+ *Cis*), 57 (MK2−), 87 (MK2− *Cis*).

(F) Immunohistochemistry of one representative MK2+ (top) and one MK2− (bottom) tumor from the same *MK2*$^{CV/CV}$;*Kras*$^{LSL\text{-}G12D/+}$;*p53*$^{flox/flox}$ mouse after cisplatin treatment as described in (E). CC3-positive cells, brown staining (arrows); scale bar represents 50 μm. Insert: serial section with MK2 staining of the same tumor region. MK2-positive stromal cells cause brown staining in the MK2− tumor.

(G) Number of CC3-positive cells/mm^2 of tumor area in *Kras*$^{G12D/+}$;*p53*$^{+/+}$ lung tumors. n = 3 mice/condition; error bars represent SEM; n (tumors) = 129 (MK2+), 116 (MK2+ *Cis*), 55 (MK2−), 27 (MK2− *Cis*).

In order to directly compare MK2-proficient and MK2-deficient tumor cells within a single animal, we created a new genetically engineered mouse model in which the gene of interest could be reversibly deactivated in vivo. By combining the MK2 Cre-versible or *MK2*^{CV} allele with an autochthonous model of NSCLC, we are able to study MK2 synthetic lethality with genetic mutations that promote tumor progression and with the response of tumor cells to genotoxic treatment in an internally controlled setting in vivo. This method should be generally applicable to study other genes in the context of synthetic lethality with anticancer agents in otherwise genetically identical solid tumors in situ within individual animals.

We found that MK2-deficient tumors were detected at the expected rate early after tumor induction and formed at the same latency as MK2-proficient tumors independent of their p53 status. In p53-deficient tumor cells, we paradoxically observed both an increase in basal apoptosis and an enhancement of proliferation in the absence of exogenous DNA damage. The increased tumor burden that was seen in MK2/p53-DKO autochthonous tumors over time indicates that enhanced proliferation rather than apoptosis dominates the phenotype. Similar results were also seen in murine xenografts from *H-Ras*^{G12V}-transformed p53-deficient MEFs when progressively monitored over time (Reinhardt et al., 2007). Faster cell doubling times seen in both murine and human MK2/p53-DKO NSCLC cell lines in vitro are likely caused by an MK2-dependent loss of cell-cycle delay following oncogenic stress. However, in contrast to what is observed for other checkpoint kinases, like ATM or Chk2 (Negrini et al., 2010), there are no data suggesting that MK2 expression is frequently lost in human tumors, suggesting that its function as a regulator of proliferation is incompletely understood in this context. In this regard, the absence of MK2 mutations in human

tumors and the lack of a correlation between expression of MK2 and p53 are similar to that of Chk1 (Figure S4).

In recent years, there has been increasing effort to target MK2 as a promising candidate for several inflammatory diseases (Fyhrquist et al., 2010; Gaestel et al., 2009). Different inhibitors for MK2 have been developed and are currently under investigation in animal models (Rao et al., 2012; Xiao et al., 2013). Emerging data about the role of MK2 in the DNA damage response, and particularly its synthetic lethal interaction with the loss of p53 after genotoxic stress, strongly suggest that testing of these compounds should be extended to include combination therapies with DNA-damaging agents in anticancer treatments.

EXPERIMENTAL PROCEDURES

Generation of MK2 Cre-Versible Mice

To generate mice carrying Cre-versible alleles of MK2, we constructed the targeting vector (Figure 1A) using standard cloning approaches (see Supplemental Experimental Procedures). Homocygous $MK2^{CV/CV}$ and $MK2^{+/+}$ mice were crossed with $Kras^{LSL\text{-}G12D/+}$;$p53^{fl/fl}$ mice (Jackson et al., 2005) from the laboratory of Tyler Jacks (MIT) to obtain $MK2^{CV/CV}$ or $MK2^{+/+}$;$Kras^{LSL\text{-}G12D/+}$;$p53^{flox/flox}$ and $MK2^{CV/CV}$ *or* $MK2^{+/+}$;$Kras^{LSL\text{-}G12D/+}$;$p53^{+/+}$ mutant mice.

All mice were maintained on a mixed C57/BL/6J x 129SvJ strain. All mouse studies described in this proposal were approved by the MIT Institutional Committee for Animal Care and conducted in compliance with the Animal Welfare Act regulations and other federal statutes relating to animals and experiments involving animals and adhere to the principles set forth in the Guide for the Care and Use of Laboratory Animals, National Research Council, 1996 (Institutional Animal Welfare Assurance No. A-3125–01).

Tumor Initiation and Cisplatin Treatment

Mice were infected with 2.5×10^7 plaque-forming units of adenovirus expressing Cre-recombinase (Ad5CMVCre; University of Iowa) by intratracheal administration (DuPage et al., 2009). Mice were given freshly prepared cisplatin in PBS at 5 mg/kg bodyweight i.p. at weeks 12, 13, and 14 after tumor initiation. The experimental endpoint was determined by weight loss of tumor-bearing animals (20% of starting body weight). For measurement of CC3-positive cells, mice were given a single dose of 10 mg/kg bodyweight i.p. 48 hr prior to sacrifice.

Immunohistochemical Analysis and Quantification

For immunohistochemistry (IHC), see the Supplemental Experimental Procedures. Tumor areas and CC3-positive cells per mm^2 were analyzed using BioQuant software. For the quantification of tumor areas, ten fields of view in different lobes of each mouse were analyzed at 10× magnification.

Doubling Times

After cisplatin (5 μM) or vehicle treatment for 4.5 hr, cells were plated in duplicates at 50,000 cells per well in a 6-well dish and cell numbers were counted every 24 hr for a total of 72 hr. Doubling times were calculated by exponential regression.

Clonogenic Survival Assay

After treatment with vehicle, 5 μM, or 10 μM cisplatin for 4.5 hr, cells were plated in triplicates at a concentration of 2,000 cells for mock-treated and 5,000 or 10,000 cells for cisplatin-treated per well in a 6-well dish. After 8 days, cells were fixed and stained with modified Wright stain (Sigma-Aldrich). Colonies consisting of >50 cells were counted; surviving fractions were determined by normalization against untreated cells.

For additional methods, primer sequences used in Southern blots, genotyping and cDNA sequencing, and antibodies and chemicals, see the Supplemental Experimental Procedures.

SUPPLEMENTAL INFORMATION

Supplemental Information includes Supplemental Experimental Procedures and four figures and can be found with this article online at http://dx.doi.org/10.1016/j.celrep.2013.10.025.

ACKNOWLEDGMENTS

We thank members of the Yaffe and Jacks labs for helpful advice and discussions and R.T. Bronson (Tufts University) for histopathology. We thank M. Gaestel (Medical School Hannover); M.A. Kerenyi (TCH Harvard); and the Swanson Biotechnology Center, especially the Ripple ES/Transgenics Facility, the Hope Babette Tang (1983) Histology Facility, and the Biopolymers and Proteomics Core Facility at the Koch Institute/MIT. This work was supported by the Austrian Science Fund (FWF) (J 2900-B21) to S.M.; NIH grants (ES015339, GM60594, GM59281, and CA112967), Janssen Pharmaceutical (Transcend), and the Koch Institute and Center for Environmental Health Sciences Core Grants (P30-CA14051 and ES-002109) to M.B.Y.; the Volkswagenstiftung (Lichtenberg Program), the Deutsche Forschungsgemeinschaft (SFB-832/A21, KFO-286/RP2, RE2246/2-1), the Ministry for Science and Technology, NRW (313-005-0910-0102), and Deutsche Jose Carreras Leukämie Stiftung (DJCLS R12/26) to H.C.R.; and the Anna Fuller Fund to I.G.C. A.D.C. is an employee of Cell Signaling Technology. The authors wish to dedicate this paper to the memory of Officer Sean Collier for his caring service to the MIT.

Received: June 6, 2013
Revised: September 10, 2013
Accepted: October 14, 2013
Published: November 14, 2013

REFERENCES

Azzoli, C.G., Baker, S., Jr., Temin, S., Pao, W., Aliff, T., Brahmer, J., Johnson, D.H., Laskin, J.L., Masters, G., Milton, D., et al.; American Society of Clinical Oncology (2009). American Society of Clinical Oncology Clinical Practice Guideline update on chemotherapy for stage IV non-small-cell lung cancer. J. Clin. Oncol. *27*, 6251–6266.

Cannell, I.G., Kong, Y.W., Johnston, S.J., Chen, M.L., Collins, H.M., Dobbyn, H.C., Elia, A., Kress, T.R., Dickens, M., Clemens, M.J., et al. (2010). p38 MAPK/MK2-mediated induction of miR-34c following DNA damage prevents Myc-dependent DNA replication. Proc. Natl. Acad. Sci. USA *107*, 5375–5380.

Ciccia, A., and Elledge, S.J. (2010). The DNA damage response: making it safe to play with knives. Mol. Cell *40*, 179–204.

DuPage, M., Dooley, A.L., and Jacks, T. (2009). Conditional mouse lung cancer models using adenoviral or lentiviral delivery of Cre recombinase. Nat. Protoc. *4*, 1064–1072.

Fyhrquist, N., Matikainen, S., and Lauerma, A. (2010). MK2 signaling: lessons on tissue specificity in modulation of inflammation. J. Invest. Dermatol. *130*, 342–344.

Gaestel, M., Kotlyarov, A., and Kracht, M. (2009). Targeting innate immunity protein kinase signalling in inflammation. Nat. Rev. Drug Discov. *8*, 480–499.

Jackson, E.L., Willis, N., Mercer, K., Bronson, R.T., Crowley, D., Montoya, R., Jacks, T., and Tuveson, D.A. (2001). Analysis of lung tumor initiation and progression using conditional expression of oncogenic K-ras. Genes Dev. *15*, 3243–3248.

Jackson, E.L., Olive, K.P., Tuveson, D.A., Bronson, R., Crowley, D., Brown, M., and Jacks, T. (2005). The differential effects of mutant p53 alleles on advanced murine lung cancer. Cancer Res. *65*, 10280–10288.

Johnson, L., Mercer, K., Greenbaum, D., Bronson, R.T., Crowley, D., Tuveson, D.A., and Jacks, T. (2001). Somatic activation of the K-ras oncogene causes early onset lung cancer in mice. Nature *410*, 1111–1116.

Lord, C.J., and Ashworth, A. (2012). The DNA damage response and cancer therapy. Nature *481*, 287–294.

Manke, I.A., Nguyen, A., Lim, D., Stewart, M.Q., Elia, A.E., and Yaffe, M.B. (2005). MAPKAP kinase-2 is a cell cycle checkpoint kinase that regulates the G2/M transition and S phase progression in response to UV irradiation. Mol. Cell *17*, 37–48.

Morandell, S., and Yaffe, M.B. (2012). Exploiting synthetic lethal interactions between DNA damage signaling, checkpoint control, and p53 for targeted cancer therapy. Prog. Mol. Biol. Transl. Sci. *110*, 289–314.

Negrini, S., Gorgoulis, V.G., and Halazonetis, T.D. (2010). Genomic instability—an evolving hallmark of cancer. Nat. Rev. Mol. Cell Biol. *11*, 220–228.

Rao, A.U., Xiao, D., Huang, X., Zhou, W., Fossetta, J., Lundell, D., Tian, F., Trivedi, P., Aslanian, R., and Palani, A. (2012). Facile synthesis of tetracyclic azepine and oxazocine derivatives and their potential as MAPKAP-K2 (MK2) inhibitors. Bioorg. Med. Chem. Lett. *22*, 1068–1072.

Reinhardt, H.C., Aslanian, A.S., Lees, J.A., and Yaffe, M.B. (2007). p53-deficient cells rely on ATM- and ATR-mediated checkpoint signaling through the p38MAPK/MK2 pathway for survival after DNA damage. Cancer Cell *11*, 175–189.

Reinhardt, H.C., Jiang, H., Hemann, M.T., and Yaffe, M.B. (2009). Exploiting synthetic lethal interactions for targeted cancer therapy. Cell Cycle *8*, 3112–3119.

Reinhardt, H.C., Hasskamp, P., Schmedding, I., Morandell, S., van Vugt, M.A., Wang, X., Linding, R., Ong, S.E., Weaver, D., Carr, S.A., and Yaffe, M.B. (2010). DNA damage activates a spatially distinct late cytoplasmic cell-cycle checkpoint network controlled by MK2-mediated RNA stabilization. Mol. Cell *40*, 34–49.

Rusch, V., Klimstra, D., Venkatraman, E., Oliver, J., Martini, N., Gralla, R., Kris, M., and Dmitrovsky, E. (1995). Aberrant p53 expression predicts clinical resistance to cisplatin-based chemotherapy in locally advanced non-small cell lung cancer. Cancer Res. *55*, 5038–5042.

Tronche, F., Casanova, E., Turiault, M., Sahly, I., and Kellendonk, C. (2002). When reverse genetics meets physiology: the use of site-specific recombinases in mice. FEBS Lett. *529*, 116–121.

Viktorsson, K., De Petris, L., and Lewensohn, R. (2005). The role of p53 in treatment responses of lung cancer. Biochem. Biophys. Res. Commun. *331*, 868–880.

Xiao, D., Palani, A., Huang, X., Sofolarides, M., Zhou, W., Chen, X., Aslanian, R., Guo, Z., Fossetta, J., Tian, F., et al. (2013). Conformation constraint of anilides enabling the discovery of tricyclic lactams as potent MK2 non-ATP competitive inhibitors. Bioorg. Med. Chem. Lett. *23*, 3262–3266.